RES MILITARIS
REVUE EUROPEENNE D ETUDES EUROPEAN JOURNAL OF MILITARY STUDIES
Social Science Journal

Residual Stress Analysis on a Fractured Double Drive Shaft Assemble – Tarantula Panser

By

Wawan Rukmono
Faculty of Defense Technology, Indonesia Defense University, Bogor, Indonesia
Email: wawansmata@idu.ac.id

Purnomo Yusgiantoro
Faculty of Defense Technology, Indonesia Defense University, Bogor, Indonesia
Email: pyc@pycenter.org

Sovian Aritonang
Faculty of Defense Technology, Indonesia Defense University, Bogor, Indonesia
Email: Sovian.aritonang@idu.ac.id

Jupriyanto
Faculty of Defense Technology, Indonesia Defense University, Bogor, Indonesia
Email: jupriyanto@idu.ac.id

Nono Darsono
Research Center for Metallurgy and Materials - LIPI, Puspiptek, Serpong 15314, Indonesia
Email: nono.dasono@lipi.ac.id

Toto Sudiro
Research Center for Physics - LIPI, Puspiptek, Serpong 15314, Indonesia
Email: toto.sudiro@lipi.go.id

Maykel Manawan
Faculty of Defense Technology, Indonesia Defense University, Bogor, Indonesia
Email: maykeltem@gmail.com

Abstract

The level of residual stresses is of great importance for many applications. In this work, the XRD residual stress analysis was used to characterize 'double drive shaft assemble' to find if it's the cause of the failure. The highest stress levels were found in the heat treat or mechanically machined specimen, while considered negligible stresses along transfers direction. In addition, shear stress and texture are observed in the $\sin^2 \psi$ – strain curve. Further results and discussion are presented in this study.

Keywords: steel, residual stress, shear stress.

1 Introduction

Combat vehicles in the defense system must have locomotion, firepower, and shock power, as well as high attack resistance (Pusat Kesenjataan Kavaleri, 2013; Pratomo et al., 2021; NATO, 2012). The criteria for carrying out defense and security operations are maneuvering speed, high cruising range, fire resistance, firepower, and protecting and transporting personnel and their logistics (Vennik, 2019; Pratomo et al., 2020).

Infracore Black Fox is one of the armored fighting vehicles made in South Korea with 90 mm caliber canons, amphibious capability, and tires to cruise on off-road and flat terrain that meets military standards (KDIA, 2019). Indonesia first ordered the Infracore Black Fox and renamed Panzer Tarantula, which has been operational since 2013 (SIPRI, 2012).

In recent years, several accidents during operation have occurred due to the failure in motion and direction control rod (double drive shaft assemble). This accident is also happened elsewhere, which caused the system to be unable to move and control its direction (Bayrakceken, Tasgetiren, and Yavuz, 2007). A material test is needed to find the cause of the failed component, such as elemental analysis, hardness, and surface residual stress.

During the manufacturing process, residual stresses are introduced into parts by heat treatment, grinding, welding, electroplating, shot blasting, or other processes (Withers and Bhasedia, 2001; Finch, 1994; Noyan, 1991). If residual stresses are large enough, the local deformation and plastic deformation can seriously affect component performance. In general, surface tensile stresses are undesirable because they can cause fatigue fracture, chill cracking, and stress-corrosion cracking. In contrast, compressive residual stresses are beneficial due to the increased resistance to fatigue and stress-corrosion cracking and the bending strength of brittle ceramics and glass (Withers and Bhasedia, 2001; Finch, 1994; Noyan, 1991; Kandil et al., 2001; Fitzpatrick et al., 2005). There are plenty of methods for measuring residual stresses, and one of the most important is the X-ray diffraction method, which, despite its limited depth of penetration, allows more accurate analysis of non-destructive residual stresses (Resigen et.al, 2017; Khorsan et al., 2017; Ogawa et al., 2019). This study aims to investigate whether residual stress contributes to the failure of ‘double drive shaft assemble’.

2 Experimental Method

The ‘double drive shaft assemble’ specimen are used to characterize the composition, hardness, and residual stress. Optical Emission Spectroscopy from Hitachi Hi-Tech is used to characterize the chemical composition of the failed specimen. Rockwell Hardness Tester from Future Tech is used to characterize the hardness of failed specimen. Bruker D8 Advance Eco diffractometer is used to characterize the material and the surface residual stress of a good specimen perpendicular to the failure direction. XRD data were obtained using Co source that operates at 1 kW (40 kV, 25 mA), with divergence slit 1°, primary and secondary soller slit 2.5°, no Kβ filter and LYNXEYE-XET detector.

The full scan is collected in 2θ range 40° - 130° step size of 0.02°, further analysis with Bruker Eva v5 and Topas v6 for the qualitative and quantitative analysis, respectively (Bruker AXS, 2019; Bruker AXS, 2017). The best peak criterion is based on Rietveld refinement results and visual inspection of the final fitting.

Residual stress diffraction patterns are collected in the 2θ range 96.5° - 102.5° step size of 0.02° and tilt angle (ψ) range -20° - +20° step size of 4°, and azimuth angle (φ) range 0° - 90° step size of 45°. DIFFRAC.Leptos v7 is employed to process the data with the following steps; background correction, polarization correction, and $K_{\alpha 2}$ stripping (Bruker AXS, 2009). Corrected peak than evaluate using gravity, parabolic, pseudo-Voigt, and Pearson-VII (Bruker AXS, 2009). The “$\sin^2\psi$ – method” of X-ray diffraction was used to study the surface residual stress based on the fundamental equation of the theory of elasticity for deformation in arbitrary direction (Withers and Bhasedia, 2001; Finch, 1994; Noyan, 1991; Kandil et al., 2001; Fitzpatrick et al., 2005):

$$\varepsilon_{\varphi\psi} = ½S_2(\sigma_{11}cos^2\varphi + \sigma_{22}sin^2\varphi + \sigma_{12}sin2\varphi - \sigma_{33})\, sin^2\psi + ½S_2(\sigma_{13}cos\varphi + \sigma_{23}sin\varphi)\, sin2\psi + S_1(\sigma_{11} + \sigma_{22}) + (½S_2 + S_1)\,\sigma_{33} \quad (1)$$

where $\varepsilon_{\varphi\psi}$ is measured strain in direction of the netplane-normal $n_{\varphi\psi}$ of the (*hkl*)-netplanes, $½s_2$ and s_1 is material-(*hkl*) and (*hkl*)-dependent elastic constants; also dependent on texture, if present, σ_{ik} is normal ($i = k$) and shear ($i \neq k$) stress components of the stress tensor. In case of linear $\varepsilon_{\varphi\psi}$ - $sin^2\psi$ function, normal stress without shear stress ($\sigma_{13} = 0$ and $\sigma_{23} = 0$) and small penetration depth of x-rays ($\sigma_{33} = 0$), equation (1) reduce to:

$$\varepsilon_{\varphi\psi} = ½S_2(\sigma_{11}cos^2\varphi + \sigma_{22}sin^2\varphi + \sigma_{12}sin2\varphi)\, sin^2\psi + S_1(\sigma_{11} + \sigma_{22}) \quad (2)$$

Figure 1a shows the residual stress measurement in a laboratory-type goniometer, where the θ scan are parallel with the ψ and ω, perpendicular to φ and χ. As a rule of thumb, the higher the Bragg peak in 2θ scans, the more accurate in determining the Δd_{hkl}. In general practices, the NPL Guide No. 52 is suitable for steel's residual stress measurement (Fitzpatrick et al., 2005). Figure 1b shows the surface residual stress direction in the material. The θ-ψ scan dictated the stress direction in respect of the surface orientation (Fitzpatrick et al., 2005).

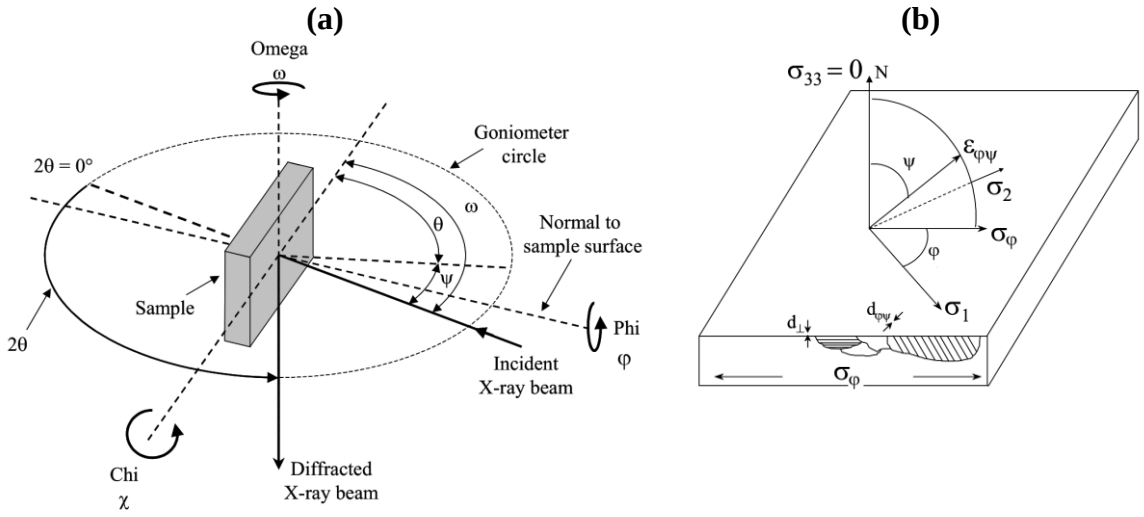

Figure 1. *Experimental setup for (a) Angles and rotations used in residual stress measurement, (b) Strain component $\varepsilon_{\varphi\psi}$ on the surface of material.*

3 Result And Discussion

Fig 1(a) shows the drive assembly sample orientation in XRD with scan area highlighted in yellow, scan direction $\varphi = 0^\circ$ (red) and $\varphi = 90^\circ$(blue). Figure 1(b) shows the Rockwell hardness testing of 120 HRB, putting the specimen in the low alloy steel category. Further, the elemental analysis in table 1 shows that the total alloy is less than 8% confirmed as low alloy steel, but the carbon content of 0.77% put this specimen in high carbon steel (0.61-1.50% at% C) with an additional 0.23% Si and 0.79% Cr to increase solid solution strength, hardness and improve corrosion/oxidation resistance (Bramfitt and Benscoter, 2001).

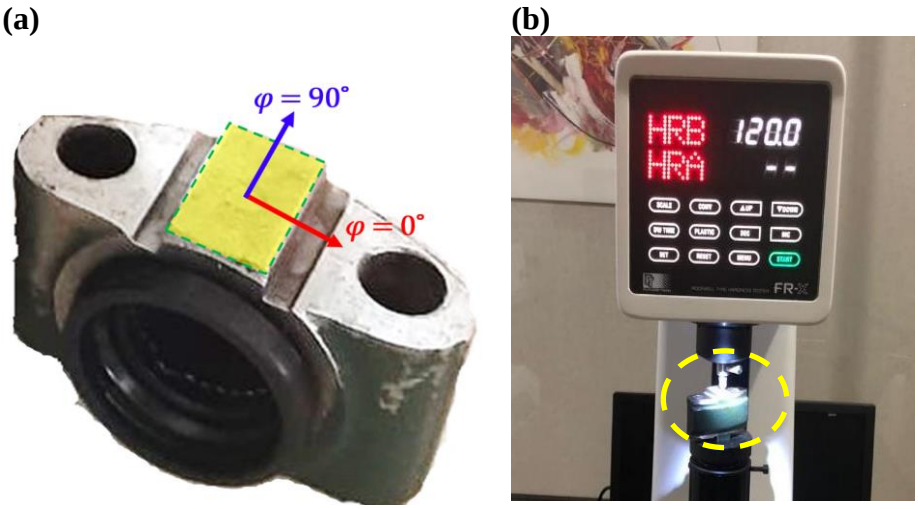

Figure 1. '*Double drive shaft assembles' in XRD setup (a) and Rockwell hardness setup (b)*

Table 1. *Chemical composition (mass%)*

	Fe	C	Si	Mn	P	S	Cr	Mo	Ni	Al	Co	Cu
Avg.	97.4	0.770	0.231	0.655	0.007	0.0030	0.789	0.0056	<0.0050	0.0136	0.0022	0.0424
SD	0.010	0.010	0.010	0.010	0.001	0.0010	0.010	0.0010	0.0010	0.0010	0.0003	0.0005

	Nb	Ti	V	W	Pb	Sn	B	Zr	As	Bi
Avg.	<0.0020	0.0014	0.042	<0.0400	<0.0150	<0.0020	<0.0010	0.0023	0.0074	0.0146
SD	0.0000	0.0002	0.005	0.0000	0.0000	0.0001	0.0001	0.0005	0.0015	0.0016

Fig. 2a shows the Rietveld refinement analysis of θ-2θ coupled scan. The sample is refined with α-Fe (ferrite) crystal structure from ICDD PDF card no. 04-007-9753 with group Im-3m. The discrepancy between observed ad calculated data are considered acceptable, shown by Goodness of Fit (GoF) of 1.13 - closer to 1.0, and expected (Rexp) and weighted value (Rwp) smaller than 10% (Manawan et al., 2021; Toby, 2006). The refinement result is summarized in Table 2.

Fig. 2b shows the ψ scan of (211)-peak using θ-2θ coupled scan. There is no change in the peak width, but the intensity decrease due to the illumination area, parallel to the scan direction, getting smaller as the tilt angle (ψ) changes from negative to positive.

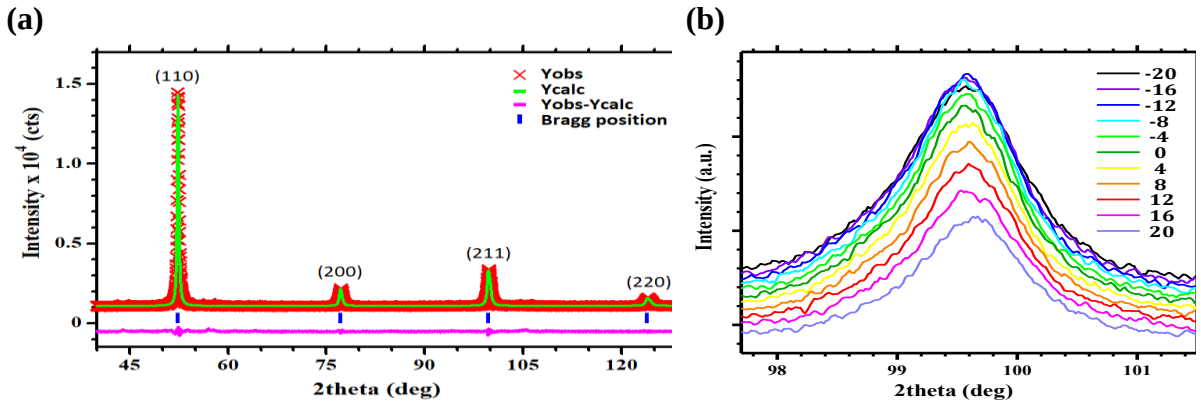

Figure 2. *X-ray diffractogram 'double drive shaft assembles' Rietveld refinement (a) and (211) residual stress scan at* $\boldsymbol{\varphi}$ *= 0° in ψ range of -20° - +20°, step size of 4° (b)*

Table 2. *Rietveld refinement result*

Phase	Steel
Space Group	Im-3m
Cell Mass	111.690(1)
Cell Volume (Å^3)	23.538 (2)
Crystal Density (g/cm^3)	7.897(1)
Lattice Parameters: *a* (Å)	2.86589 (7)
Rexp	5.22
Rwp	5.92
GoF	1.13

A total of eleven data of each azimuth angle (φ) was reduced, fitted, and evaluated by $\sin^2\psi - \sigma$ plot as shown in Fig. 3. All curves show a negative slope indicating compressive stress and an elliptical function indicating shear stress. There is no significant change in the slope as the specimen rotates from $\varphi = 0^\circ$ to $\varphi = 90^\circ$ which mean that the strain is isotropic.

Table 3 summarizes the strain analysis from $\mathrm{Sin}^2\psi$ - σ plot where the highest compressive stress is at $\varphi = 0°$ and the lowest is at $\varphi = 90°$ with the value of -295.3 MPa and -275.9 MPa, respectively. This value is similar to quenched decarburizing silicon-manganese suspension springs for automotive application (Todinov, 2000; Lozano, 2019). The error value is quite high due to the presence of texture, which is seen as an oscillation of individual data compared to the fitting. Shear stress follows the normal stress pattern with the value of -47.5 Mpa for $\varphi = 0°$ and -44.8 MPa $\varphi = 90°$, respectively.

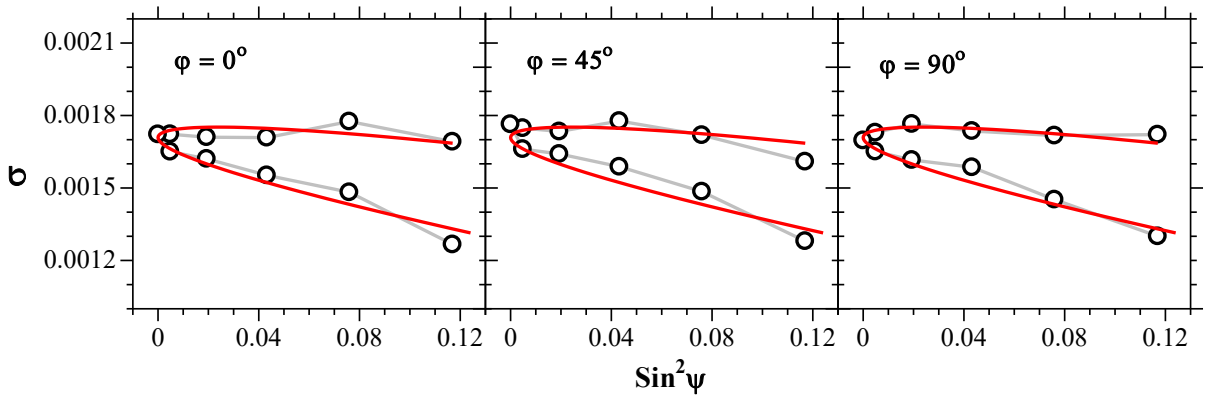

Figure 3. *$\mathrm{Sin}^2\psi$ - σ plot of surface residual stress as a function of* $\boldsymbol{\varphi}$

Table 3. *Residual stress analysis result*

φ (°)	Normal Stress (MPa)	Shear Stress (MPa)
0	-295.3 ± 53.1	-47.5 ± 5.3
45	-278.9 ± 45.4	-45.6 ± 7.2
90	-275.9 ± 49.4	-44.8 ± 6.5

Conclusion

Residual stress using "sin^2 $\boldsymbol{\psi}$ – method" has been used for failure analysis on 'double drive shaft assembles' military vehicle. The strain on the specimen was composed of compressive residual stress and shear stress with the maximum value of -295.3 MPa and -47.5 MPa, respectively. Compresive residual stress is desirable, while shear stress is still below the

minimum tolerance for shear modulus (MatWeb, 2022). Thus, the components are free from the destructive effects of residual stress.

4 Acknowledgment

Authors would like to thank Rektor Unhan, Ka LP2M Unhan, Dekan FTP, Sesprodi TDG, P2M-LIPI, P2F-LIPI.

References

Pusat Kesenjataan Kavaleri (2013) "Buku petunjuk Induk Kecabangan Kavaleri." Manual

Pratomo, A. N. et al. (2021) "Design Optimization and Structural Integrity Simulation of Aluminum Foam Sandwich Construction for Armored Vehicle Protection." Composite Structures, 114461. https://doi.org/10.1016/j.compstruct.2021.114461.

NATO (2012) STANAG 4569 (Edition 2) -Protection levels for occupants of armoured vehicles. Standard

Vennik, K. (2019) "The Effect of Military Vehicles on Rut Formation on Estonian Soils and Natural Recovery of The Ruts." Estonian University of Life Sciences. ISBN 978-9949-629-74-9 (Thesis)

Pratomo, A. N. et al. (2020) "Countermeasures design and analysis for occupant survivability of an armored vehicle subjected to blast load." J. Mech. Sci. Technol., 34(5), 1893–1899. https://doi.org/10.1007/s12206-020-0411-1.

KDIA (2019) Korea Defense Products Guide. Catalog

SIPRI (2012) "Armaments, Disarmament and International Security." Stockholm Internasional Peace Research Institute. Magazine

Bayrakceken, H., Tasgetiren, S. and Yavuz, I. (2007) "Two cases of failure in the power transmission system on vehicles: A universal joint yoke and a drive shaft." Eng. Fail. Anal., 14(4), 716–724. https://doi.org/10.1016/j.engfailanal.2006.03.003.

Withers, P. J. and Bhadeshia, H.K.D.H. (2001) 'Residual Stress-II: Nature and Origins', Mat. Sci. Tech. 17 (366). https://doi.org/10.1179/026708301101510087

Finch, D.M. (1994) "A review of residual stress measurement methods A guide to technique selection." ERA Report 94-0101R, ERA Technology Ltd, Leatherhead, Surrey, UK.

Noyan, I. C. (1991) "Defining residual stresses in thin film structures." Adv. X-Ray Anal., 35(A), 461-473. https://doi.org/10.1154/S0376030800009149

Kandil, F., Lord, J. D., Fry, A. T. and Grant, P. (2001) "A review of residual stress measurement methods - a guide to technique selection." NPL Report MATC(A)O4.

Fitzpatrick, M.E., Fry, A.T., Holdway, P., Kandil, F.A., Shackleton, J., Suominen, L. (2005) "Determination of Residual Stresses by X-ray Diffraction." NPL Guide No. 52, UK.

Reisgen, U., Sharma, R., Gach, S., Olschok, S., Francis, J., Bobzin, K., Oete, M., Wiesner, S., Knoch, M. and Schmidt A. (2017) "Residual Stress Measurement in AlSi Alloys." Mat. Sci. Eng. Tech. 48(12), 270-1275. https://doi.org/10.1002/mawe.201700157

Khorsand, S. and Huang, Y. (2017) "Integrated Casting-Extrusion (ICE) of an AA6082 Aluminium Alloy." In: Ratvik A. (eds) Light Metals, 235-241.

Ogawa, D., Kakiuchi, T., Hashiba, K. and Uematsu, Y. (2019) "Residual stress measurement of Al/steel dissimilar friction stir weld." Sci. Technol. Weld. Join, 24 (8) https://doi.org/10.1080/13621718.2019.1588521

Bruker AXS, 2019. DIFFRAC.EVA V5.1. Bruker AXS GmbH, Karlsruhe, Germany

Bruker AXS, 2017. DIFFRAC.TOPAS V6. Bruker AXS GmbH, Karlsruhe, Germany

Bruker AXS, 2009. DIFFRAC.Leptos V7. Bruker AXS GmbH, Karlsruhe, Germany

Bramfitt, B. L. and Benscoter, A.O. (2001) "Metallographer's Guide: Practice and Procedures for Irons and Steels." ASM Int., USA

Manawan, M., Kartini, E. and Avdeev, M. (2021) "Visualizing lithium ions in Li3PO4 by neutron diffraction." J. Appl. Cryst. 54, 1409–1415. https://doi.org/10.1107/S1600576721008700

Toby, B. H. (2006) 'R factors in Rietveld analysis: How good is good enough?' Powder Diffr. 21, 67–70. https://doi.org/10.1154/1.2179804

Todinov, M.T. (2000) "Residual stresses at the surface of automotive suspension springs." J. Mater. Sci. 35, 3313–3320. https://doi.org/10.1023/A%3A1004887708822

Lozano, D.E., Totten, G.E., Bedolla-Gil, Y., Guerrero-Mata, M., Carpio, M., Martinez-Cazares G.M. (2019) "X-ray Determination of Compressive Residual Stresses in Spring Steel Generated by High-Speed Water Quenching." Mater. 12(7), 1154. https://doi.org/10.3390/ma12071154

MatWeb (2022, January 10) "Overview of materials for Low Alloy Steel." Retrieved from http://www.matweb.com